

## **Correlation of EBIC and SWBXT Imaged Defects and Epilayer Growth Pits in 6H-SiC Schottky Diodes**

C. M. Schnabel<sup>1</sup>, M. Tabib-Azar<sup>1</sup>, P. G. Neudeck<sup>2</sup>, S. G. Bailey<sup>2</sup>, H. B. Su<sup>3</sup>,  
M. Dudley<sup>3</sup>, and R.P. Raffaele<sup>4</sup>

<sup>1</sup>Case Western Reserve Univ., Glennan 517, 10900 Euclid Avenue, Cleveland, Ohio 44106, USA

<sup>2</sup>NASA Glenn Research Center, MS 77-1, 21000 Brookpark Road, Cleveland, Ohio 44135, USA

<sup>3</sup>State University of New York at Stony Brook, Stony Brook, New York 11794, USA

<sup>4</sup>Rochester Institute of Technology, Rochester, NY 14623

**Keywords:** Defects, Diffusion Length, Electron Beam Induced Current (EBIC), Epilayer Growth Pits, Recombination Centers, Screw Dislocation, Synchrotron White-Beam X-Ray Topography (SWBXT)

**Abstract:** We show the first direct experimental correlation between the presence of closed core screw dislocations in 6H-SiC epilayers with recombination centers, as well as with some of the small growth pits on the epilayer surface in lightly-doped 6H-SiC Schottky diodes. At every SWBXT-identified closed core screw dislocation, an EBIC image showed a dark spot indicating a recombination center, and Nomarski optical microscope and Atomic Force Microscope (AFM) images showed a corresponding small growth pit with a sharp apex on the surface of the epilayer.

**Introduction:** The ability to readily identify the electrical properties of an extended crystal defect in a semiconductor is paramount in determining whether the defect influences the performance of various devices. Electron-beam-induced current (EBIC) measurement using the planar mapping technique enables quantitative analysis and spatial visualization of recombination centers that reduce the diffusion length of minority carriers in 6H-SiC Schottky diodes [1,2,3]. Such a procedure coupled with synchrotron white-beam x-ray topography (SWBXT), through which closed core screw dislocations may be identified by their stress signature in the crystal lattice [4], gives insight into the effects of these defects on the minority carrier diffusion length. The SWBXT image may also be correlated to the as-grown homoepilayer surface by comparison with Nomarski optical microscopy and atomic force microscopy (AFM) images.

**Experimental Procedure:** Following the growth of a 3.5  $\mu\text{m}$  thick  $1.2 \times 10^{16} \text{ cm}^{-3}$  n-type homoepilayer on a 3.5  $\mu\text{m}$  off-axis commercial 6H-SiC substrate [5] by CVD [6], we generated a map of closed core screw dislocations using SWBXT [4]. The wafer backside was polished prior to SWBXT to ensure sufficient X-ray image quality that individual closed core screw dislocations were clearly resolvable throughout the entire sample. Following deposition and annealing of a backside Ni ohmic contact ( $\sim 925 \text{ } \mu\text{C}$ , 5 minutes in argon ambient), thin gold Schottky contacts (approx. 400  $\text{nm}$  thick) of up to 0.86 mm x 0.86 mm in area were then patterned on the epilayer surface using E-beam evaporation and lift-off photolithography. High magnification (400X) Nomarski optical images of the surface features of individual dies were made. With the assistance of AFM analysis, the observed features evident on the Au Schottky contacts were categorized as either particulates on the top surface of the Schottky metal due to sample handling, or growth pits in the as-grown epilayer observable through the thin metallization.

EBIC images were generated by raster-scanning the 25 keV electron-beam across the entirety of the die while measuring the collected current as a function of position. Lighter shades correspond

to higher collected currents indicating longer minority carrier lifetime, while areas of enhanced minority carrier recombination (i.e., lower carrier lifetime and lower collected currents) are imaged as dark spots [1]. Because raw images collected by SWBXT and EBIC were somewhat distorted, computer image processing was needed to restore raw images to the proper aspect ratio corresponding to the proper aspect ratio of the original sample. All images were digitally scanned into a computer so that the images could be undistorted, scaled, and digitally overlaid as separate image layers using the four corners of the 7.5 mm x 6 mm rectangular sample as common reference coordinates. The computer contrast enhancement of images and creation of partially transparent derived layers expedited correlation of data from all three measurements.

**Results:** The figures below illustrate the same device region showing part of a 0.86 mm x 0.86 mm Schottky diode recorded by SWBXT (Figure 1), EBIC (Figure 2), and optical microscope (Figure 3, with AFM inset of a small growth pit). All the closed core screw dislocations revealed in Figure 1 are clearly reflected by correspondingly located dark spots in the EBIC image of Figure 2. It is readily apparent, however, that there are additional dark spots in the EBIC image for which no screw dislocation is present. While less obvious in Figure 3 due to their very small size, small growth pits typical of the AFM inset were also identified at every screw dislocation. However, not all EBIC-revealed recombination centers and not all small growth pits are associated with screw dislocations. The small growth pits correlated with screw dislocations appear similar in size and shape, while those that are not associated with screw dislocation sometimes have different shapes. Some EBIC dark spots and some epilayer small growth pits appear completely independent in that they show up in none of the other images (such as RC-1 in Figure 2 and GP-1 in Figure 3). Most, but not all, growth pits unassociated with screw dislocations did not yield strong EBIC signatures. Table 1 shows the defect statistics recorded at six locations consisting of four different 860  $\mu\text{m}$  x 860  $\mu\text{m}$  diodes plus two similar-sized areas consisting of many smaller patterned Schottky contacts.

Screw dislocations significantly reduce the effective diffusion length of carriers in the sample. Figure 4 shows the diffusion length as a function of position across screw dislocation SD-1 shown in Figure 2. The diffusion length is calculated on the order of 3.4  $\mu\text{m}$  far from the defect, but drops around 30% to as low as 2.4  $\mu\text{m}$  near the center of the defect. This behavior is typical of the screw dislocations measured in this 6H-SiC sample.

Figure 5 shows the AFM sectional data plot taken through the middle of the small growth pit associated with SD-1, as illustrated by the white line in the middle of the AFM inset of Figure 3. One end of the metal-covered small growth pit consists of a sharp apex of at least 18 nm in depth. This data is typical of all the small growth pits associated with screw dislocations measured by AFM on this sample. Such sharp interface features could conceivably enhance carrier emission/leakage from the semiconductor impacting SiC Schottky diode I-V properties as well as MOS insulator reliability. Once very small area devices have been fabricated (i.e., small enough that some are free of certain defects), a comprehensive study of Schottky I-V properties as a function of imaged defects is planned. If successful, such a study might be able to conclusively link specific kinds of crystal defects to important electrical anomalies observed in the SiC Schottky diode literature (particularly Refs. [2], [7], and [8]).

## **Conclusion**

All screw dislocations result in EBIC-identified minority carrier recombination centers in the SiC epilayer, and in small growth pits at the sample surface. However, not all growth pits are due to screw dislocations. Not all minority carrier recombination centers are due to screw dislocations.

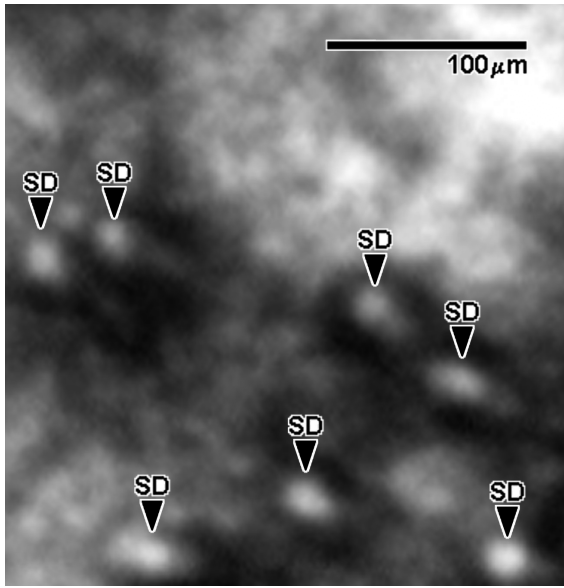


**Fig. 1.** SWBXT map of a selected diode section. The lighter spots in the image are elementary screw dislocations causing high stress regions in the crystal lattice.

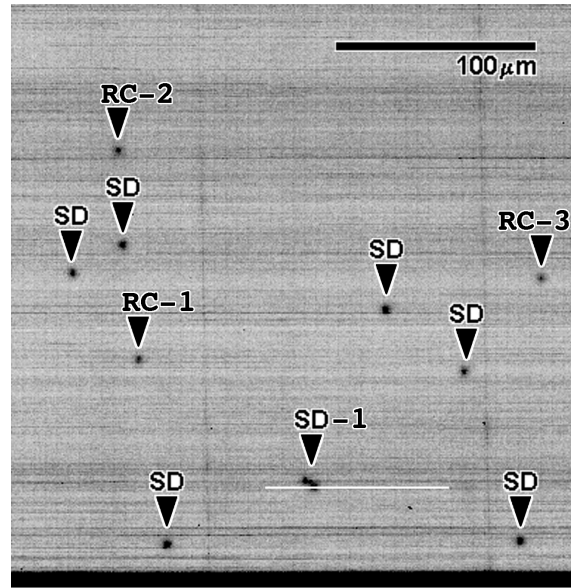


**Fig. 2.** EBIC image of a selected diode section. Darker regions indicate lower collected current, which corresponds to a reduction in the effective diffusion length.

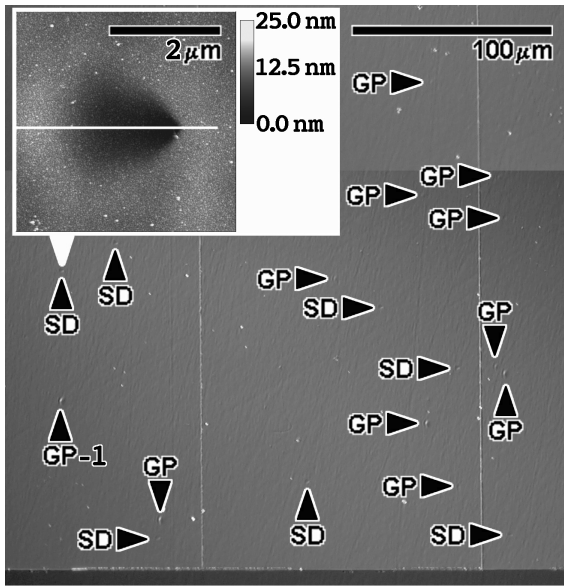


**Fig. 3.** Nomarski image of a selected diode section. Both growth pits and other particulates are evident on the sample surface. The inset shows an AFM image of a growth pit typical of a screw dislocation.

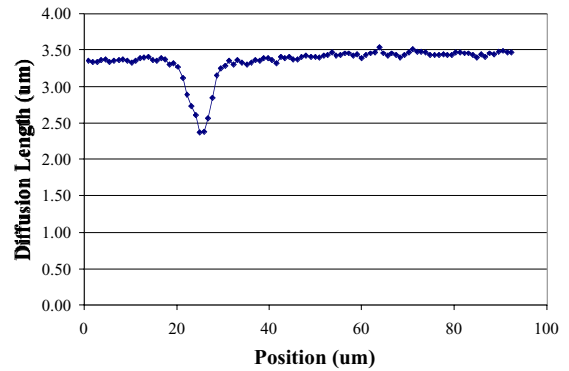


**Fig. 4.** Diffusion length as a function of position extracted from the EBIC linescan, as shown by the white line across SD-1 of Figure 2.

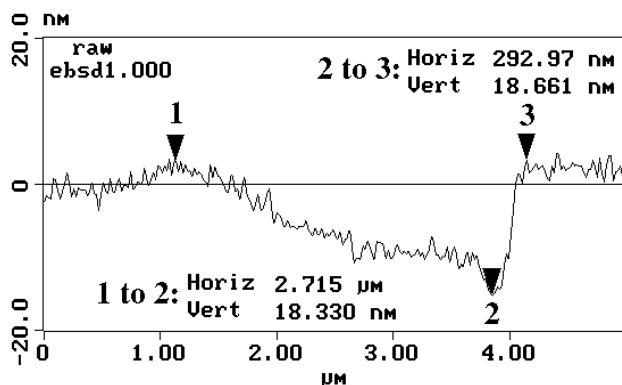


**Fig. 5.** AFM sectional data plot taken through the middle of the small growth pit associated with SD-1, as illustrated by the white line in the middle of the AFM inset of Figure 3. One end of the metal-covered small growth pit consists of a sharp apex of at least 18 nm in depth. This data is typical of all the small growth pits associated with screw dislocations measured by AFM on this sample.

**Table 1** Number of defects on different 1 mm x 1 mm dies by observation category.

Die I.D. Label on Chip ->	Bd	Dc	Db <sup>5</sup>	Df <sup>5</sup>	Ab <sup>3,5</sup>	Bc <sup>3,5</sup>
EBIC recombination centers	126	105	98	161	31	32
SWBXT identified screw dislocations over die(s) <sup>1</sup>	40	27	41	43	7	10
Nomarski identified small growth pits <sup>5</sup>	176	159	-	-	-	-
Recombination centers matching screw dislocations <sup>2</sup>	36 <sup>4</sup>	27	41	43	7	10
Growth pits matching screw dislocations <sup>2,5</sup>	40	27	-	-	-	-

1. Large areas of high stress are counted as a screw dislocation, although it may be due to many screw dislocations or another defect such as a micropipe.
2. If one growth pit or recombination center is within approx. 20 μm of the screw dislocation it is considered correlated with that screw dislocation.
3. Ab and Bc represent many smaller dies that lie close together, and therefore have much smaller measured areas than dies Bd, Dc, Db, and Df.
4. Probe tip and contact damage obscured EBIC observation of some screw dislocations.
5. Growth pit data not collected on die Db, Df, Ab, and Bc.

**Acknowledgements:** NASA Glenn: J. A. Powell, D. Larkin, C. Salupo, G. Beheim, J. Heisler, A. Trunek, L. Keys. CWRU work supported by NASA Glenn Grant NCC3-593. SUNY support from the U.S. Army Research Office under contract number DAAG559810392 (contract monitor Dr. John Prater), partially funded by the DARPA Microsystems Technology Office (Order#E111/3 monitored by Dr. Dan Radack) and NASA Glenn. Topography carried out at the NSLS, at BNL, which is supported by the U.S. Department of Energy, contract number DE-AC02-98CH10886.

## References

- [1] H. J. Leamy, J. Appl. Phys. 53 (1982), p. R51.
- [2] M. Bhatnagar, et. al., IEEE Trans. Electron Devices 43 (1996), p. 150.
- [3] M. Tabib-Azar, et. al., J. Appl. Phys. 84 (1998), p. 3986.
- [4] M. Dudley and X. Huang, this conference.
- [5] Cree Research, Inc., 4600 Silicon Drive, Durham, NC 27703.
- [6] D. J. Larkin, MRS Bulletin 22 (1997), p. 36.
- [7] R. Raghunathan and B. J. Baliga, Appl. Phys. Lett. 72 (1998), p. 3196.
- [8] D. Defives et. al., IEEE Trans. Electron Devices 46 (1999), p. 449.